Inorganic Chemistry

Article

pubs.acs.org/IC

$Ba_2AsGaSe_5$: A New Quaternary Selenide with the Novel $[AsGaSe_5]^{4-}$ Cluster and Interesting Photocatalytic Properties

Chao Li,[†,‡,§] Xiaoshuang Li,[†,‡,§] Hongwei Huang,[∥] Jiyong Yao,*[,†,‡] and Yicheng Wu[†,‡]

[†]Center for Crystal Research and Development and [‡]Key Laboratory of Functional Crystals and Laser Technology, Technical Institute of Physics and Chemistry, Chinese Academy of Sciences, Beijing 100190, People's Republic of China

[§]University of Chinese Academy of Sciences, Beijing 100049, People's Republic of China

[∥]Beijing Key Laboratory of Materials Utilization of Nonmetallic Minerals and Solid Wastes, National Laboratory of Mineral Materials, School of Materials Science and Technology, China University of Geosciences, Beijing 100083, People's Republic of China

Supporting Information

ABSTRACT: The new zero-dimensional selenide $Ba_2AsGaSe_5$ was synthesized via a solid-state reaction at 900 °C. It belongs to the orthorhombic space group *Pnma* with a = 12.632(3) Å, b = 8.9726(18) Å, c = 9.2029(18) Å, and Z = 4. In the structure, the As atom adopts trigonal-pyramidal coordination owing to the stereochemically active $4s^2$ lone pair electrons and the Ga atom is tetrahedrally coordinated with four Se atoms. The $AsSe_3$ trigonal pyramids share edges with $GaSe_4$ tetrahedra to form novel $[AsGaSe_5]^{4-}$ clusters, which are further separated from each other by Ba^{2+} cations. The optical band gap was determined as 1.39 eV according to UV−vis−NIR diffuse reflectance spectroscopy. Interestingly, the photocatalytic behavior investigated by decomposing rhodamine B indicates that the compound displays a 6.5 times higher photocatalytic activity than does P25.

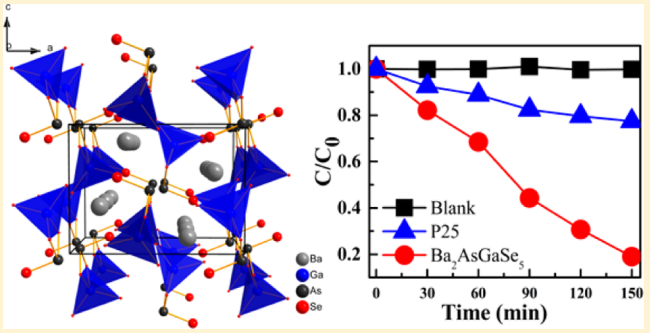

INTRODUCTION

Low-dimensional structures are of great interest due to their intriguing structures and important electrical, optical, and magnetic properties.[1−10] From a structural point of view, low-dimensional structures result from the coexistence and separation of several building units with different bonding nature (covalent, ionic, or van der Waals) in one compound. The interplay of these different bonding units gives the materials unique properties. For instance, the *Ln*FeO*Pn* (*Ln* = rare-earth metal; *Pn* = P, As) oxypnictinide superconductors contain alternately stacked ionic Ln_2O_2 layers and covalent Fe_2Pn_2 layers.[11] The electron or hole doping is achieved by varying the elements in the Ln_2O_2 layers, which may induce further change in the electronic structure of the Fe_2Pn_2 layer,. the main structural unit for the superconducting performance, thus significantly influencing the superconducting behavior. Similarly, in the *p*-type transparent conducting material *Ln*CuOTe (*Ln* = La, Ce, Nd)[12] and BaCuQF (Q = S, Se),[13] the hole conduction is realized via the covalent Cu_2Q_2 layers, which form the valence band maximum, whereas the large band gap and the high transparent quality are maintained through the ionic Ln_2O_2 or Ba_2F_2 layers confining the Cu−S bonds in the CuS layers.

In comparison with the large number of two-dimensional (2D) and one-dimensional (1D) structures, the number of zero-dimensional (0D), e.g. "molecular", inorganic compounds is much smaller. Furthermore, inorganic 0D compounds, often synthesized via high-temperature solid-state reactions, contain anions with simple structures, such as the $[BO_3]^{3-}$ triangles in Na_3BO_3[14] and $Ca_4LnO(BO_3)_3$ (*Ln* = rare-earth metal),[15] the $[AsS_3]^{3-}$ trigonal pyramids in $Pr_4As_2S_9$,[16] the $[GeCl_3]^-$ trigonal pyramids in $CsGeCl_3$,[17] the tetrahedral $[WS_4]^{2-}$ in A_2WS_4 (A = Cs, Rb)[18] and $[MSe_4]^{5-}$ in $Ba_5M_2Se_8$ (M = Al, Ga),[19] the $[Ga_2S_7]^{8-}$ anion (two tetrahedra with a common corner) in $Ba_4Ga_2S_7$,[20] the $[U_2I_{10}]^{2-}$ anion (two octahedra with a common edge) in $[Ta_7(Se_2)_{14}][U_2I_{10}]_2$,[21] and the $[B_3O_6]^{3-}$ anion (three triangles with three common corners) in the commercial NLO crystal β-BaB_2O_4 (BBO).[22] In recently years, many interesting and more complex anions have been discovered as a result of the development of the synthesis methods.[23] For example, the novel uranyl sulfide $Na_2Ba_2(UO_2)S_4$[24] comprises isolated centrosymmetric $[(UO_2)S_4]^{6-}$ anions that are surrounded by Na^+ and Ba^{2+} cations and $Cs_5[U_2(\mu\text{-}S_2)_2Cl_8]I$[25] contains the $[U_2(\mu\text{-}S_2)_2Cl_8]^{4-}$ anion with two US_4Cl_4 square antiprisms sharing two common S_2^{2-} anions, while $Cs_5P_5Se_{12}$[26] contains $[P_5Se_{12}]^{5-}$ anions featuring an octahedrally coordinated P^{3+} cation surrounded by two ethane-like $[P_2Se_6]^{4-}$ units and exhibits a second harmonic generation response.

In the search for new As-containing chalcogenides, we discovered a 0D quaternary selenide, namely $Ba_2AsGaSe_5$, through a solid-state reaction.[27] It displays discrete unprece-

Received: July 4, 2015
Published: September 29, 2015

DOI: 10.1021/acs.inorgchem.5b01501
Inorg. Chem. 2015, 54, 9785−9789

dented $[AsGaSe_5]^{4-}$ anions consisting of edge-shared $GaSe_4$ tetrahedra and $AsSe_3$ trigonal pyramids. Furthermore, inspired by the research that many compounds containing cations with electron lone pairs demonstrate excellent photocatalytic activities,[28−30] we studied the photocatalytic performance of $Ba_2AsGaSe_5$. Interestingly, the compound exhibits a photocatalytic activity to RhB about 6.5 times that of P25.

EXPERIMENTAL SECTION

Syntheses. All elements, including Ba (3N), As (4N), Ga (5N), and Se (6N), were obtained from Sinopharm Chemical Reagent Co., Ltd., and used without further purification. BaSe, As_2Se_3, and Ga_2Se_3 were first synthesized by traditional solid-state reactions of the elements in sealed silica tubes at temperatures of 620, 450, and 980 °C, respectively.

Crystal Growth of $Ba_2AsGaSe_5$. A mixture of 0.5 mmol of BaSe, 0.125 mmol of As_2Se_3, and 0.125 mmol of Ga_2Se_3 was ground in a glovebox and loaded into a fused-silica tube. The tube was then evacuated to a high vacuum of 10^{-3} Pa atmosphere and sealed. Afterward, the sample was heated in a resistance furnace to 900 °C in 15 h and kept at that temperature for 48 h. After the reaction, the sample was slowly cooled at 3 °C/h to 350 °C, and then the furnace was shut off. The resultant air-stable chip black crystals were manually selected for structure characterization. Elemental analysis of the crystals was performed on an EDX-equipped Hitachi S-4800 SEM instrument, and the results showed that the crystals consisted of Ba:As:Ga:Se in a molar ratio of 2:0.95:0.96:4.78.

A polycrystalline $Ba_2AsGaSe_5$ sample was synthesized by a stoichiometric high-temperature reaction. A 0.531 g portion of BaSe, 0.238 g of As_2Se_3, and 0.231 g of Ga_2Se_3 were ground and loaded into a fused silica tube in a glovebox. The sample was sealed under 10^{-3} Pa vacuum and heated at 800 °C for 48 h. X-ray powder diffraction analysis in the range 2θ = 10−70° with a 0.02° scan step width and a 0.1 s/step counting time was performed with the use of an automated Bruker D8 X-ray diffractometer equipped with Cu Kα (λ = 1.5418 Å) radiation. Figure 1 shows the XRD pattern of the polycrystalline

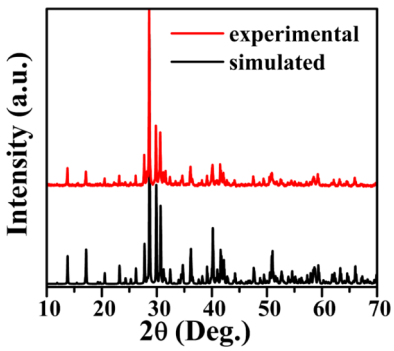

Figure 1. Experimental (red) and simulated (black) X−ray powder diffraction patterns of $Ba_2AsGaSe_5$.

$Ba_2AsGaSe_5$ sample along with the simulated pattern according to the single-crystal crystallographic data. The experimental pattern agrees with the calculated pattern except for a tiny extra peak at 22.5° belonging to GaSe.

Structure Determination. Single-crystal X-ray diffraction data were collected at 153 K on a Rigaku AFC10 diffractometer (Mo Kα, λ = 0.71073 Å). The program CrystalClear[31] was used for the data collection, cell refinement, and data reduction. Face-indexed absorption corrections were performed with the program XPREP.[32]

The structure was solved with the direct methods program SHELXS and refined with the least-squares program SHELXL of the SHELXTL.PC suite of programs.[32] Anisotropic displacement parameters and a secondary extinction correction were included in the final refinement. Tables 1−3 give additional experimental details and selected metrical data. Further details may be found in the Supporting Information.

Table 1. Crystal Data and Structure Refinement Details for $Ba_2AsGaSe_5$

fw	814.12
a (Å)	12.632(3)
b (Å)	8.9726(18)
c (Å)	9.2029(18)
space group	*Pnma*
V (Å^3)	1043.1(4)
Z	4
T (K)	153.15
λ (Å)	0.71073
ρ_c (g/cm^3)	3.122
μ (cm^{-1})	30.552
$R(F)^a$	0.0422
$R_w(F_o^2)^b$	0.0874

$^aR(F) = \sum||F_o| - |F_c||/\sum|F_o|$ for $F_o^2 > 2\sigma(F_o^2)$. $^bR_w(F_o^2) = \{(\sum[w(F_o^2 - F_c^2)^2]/\sum wF_o^4\}^{1/2}$ for all data; $w^{-1} = \sigma^2(F_o^2) + (zP)^2$, where $P = (\mathrm{Max}(F_o^2,0) + 2F_c^2)/3$.

Table 2. Selected Bond Lengths (Å) and Bond Angles for $Ba_2AsGaSe_5$

Ba−Se1	3.435(1)	Ba−Se4	3.380(1)
Ba−Se1	3.458(1)	Ba−Se4	3.396(1)
Ba−Se2	3.386(1)	As−Se1 × 2	2.463(5)
Ba−Se2	3.414(1)	Ga−Se1 × 2	2.438(2)
Ba−Se3	3.407(1)	Ga−Se2	2.353(5)
Ba−Se3	3.344(1)	Ga−Se3	2.370(1)
As−Se4	2.393(6)		
Se1−As−Se1	95.99(1)	Se1−Ga−Se3 × 2	110.96(8)
Se1−As−Se4 × 2	98.659(3)	Se2−Ga−Se3	111.44(5)
Se1−Ga−Se1	97.32(1)	As−Se1−Ga × 2	82.97(1)
Se1−Ga−Se2 × 2	112.70(1)		

Diffuse Reflectance Spectroscopy. The diffuse reflectance spectrum of $Ba_2AsGaSe_5$ was measured on a Cary 5000 UV−vis−NIR spectrophotometer with a $BaSO_4$ plate used as a reference material (100% reflectance). The optical absorption spectra were converted from diffuse reflectance spectra using the Kubelka−Munk function,[33] $\alpha/S = (1 - R)^2/2R$, where R is the diffuse reflectance and α and S are the Kubelka−Munk absorption and scattering coefficients.

Photocatalytic Activity Experiment. The organic dye molecule Rhodamine B (RhB) was selected as the degradation model to investigate the photocatalytic activity. In a typical photodegradation process, 50 mg of photocatalyst was dispersed into 50 mL of 3×10^{-5} mol/L RhB aqueous solution. Before the light was turned on, the mixture was strongly stirred for 0.5 h in the dark to achieve an adsorption−desorption equilibrium between the RhB and the photocatalysts. Then, the suspensions were exposed to a 1000 W Xe lamp coupled with 420 filters (λ >420 nm). At appropriate intervals, 5 mL of the suspension was collected and centrifuged at 5000 rpm for 10 min to remove the solid. Finally, the RhB concentration was measured on a UV-5500 PC spectrophotometer according to the absorption band of 554 nm. A P25 sample was used as a reference under the same conditions.

RESULTS AND DISCUSSION

Crystal Structure. $Ba_2AsGaSe_5$ belongs to the orthorhombic centrosymmetric space group *Pnma* with unit cell parameters a = 12.632(3) Å, b = 8.9726(18) Å, c = 9.2029(18) Å, and Z = 4. As shown in Table 3, there is one crystallographically unique Ba atom, one independent Ga atom,

DOI: 10.1021/acs.inorgchem.5b01501
Inorg. Chem. 2015, 54, 9785−9789

Table 3. Positional Coordinates and Equivalent Isotropic Displacement Parameters for $Ba_2GaAsSe_5$

atom	Wyckoff	symmetry	*x*/*a*	*y*/*b*	*z*/*c*	U_{eq} (Å^2)
Ba	8*d*	1	0.17459(3)	−0.00594(4)	0.36791(4)	0.00454(11)
Ga	4*c*	*m*	0.09704(8)	0.2500	0.66405(11)	0.0045(2)
As	4*c*	*m*	0.03643(8)	0.2500	1.00693(10)	0.00547(19)
Se1	8*d*	1	0.05637(5)	0.04598(7)	0.82990(7)	0.00514(14)
Se2	4*c*	*m*	0.01154(7)	−0.2500	0.54377(10)	0.00496(18)
Se3	4*c*	*m*	0.27893(7)	0.2500	0.60087(10)	0.00493(18)
Se4	4*c*	*m*	0.21239(7)	0.2500	0.10344(10)	0.00513(18)

one independent As atom, and four independent Se atoms (Se1−Se4) in the asymmetric unit. Se1 and Ba are at Wyckoff positions 8*d*, while the other atoms occupy the 4*c* position. The oxidation states for Ba, Ga, As, and Se are 2+, 3+, 3+, and 2−, respectively.

Figure 2 illustrates the coordination environment of the metal cations. The Ba^{2+} cations are surrounded by a bicapped

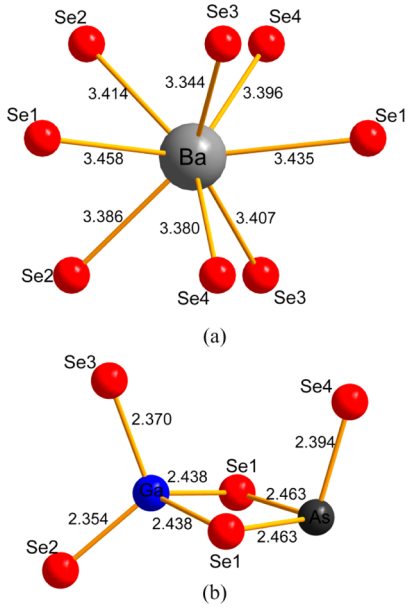

Figure 2. (a) Coordination environment of Ba. (b) Structure of the $[GaAsSe_5]^{4-}$ anion (bond lengths are given in Å).

trigonal prism of eight Se atoms with the Ba−Se distances ranging from 3.344(1) to 3.458(1) Å, which are comparable to those of 3.409(2)−3.873(1) Å in $BaAl_4Se_7$,[34] 3.261(6)−3.740(6) Å in $Ba_2As_2Se_5$,[35] 3.228(1)−3.770(1) Å in $Ba_6Sn_6Se_{13}$,[36] and 3.366(1)−3.509(1) Å in $Ba_2SbGaSe_5$.[37] Owing to the stereochemical activity of the $4s^2$ electron lone pair, the As^{3+} cations are trigonal pyramidally coordinated to three Se atoms. The As−Se distances within the $AsSe_3$ trigonal pyramid change from 2.393(6) to 2.463(5) Å, and the Se−As−Se bond angles vary from 95.99(1) to 98.659(3)°. Such values are normal, as shown in $Ba_2As_2Se_5$, which has As−Se distances of 2.357(6)−2.554(7) Å and Se−As−Se bond angles of 86.712(2)−106.425(2)°. Ga connects with four Se atoms to form a tetrahedron with Ga−Se lengths varying from 2.353(3) to 2.438(2) Å, consistent with those of 2.362(2)−2.488(2) Å in $BaGa_4Se_7$, and 2.346(2)−2.438(1) Å in $Ba_2SbGaSe_5$.

As shown in Figure 3, the crystal adopts a zero-dimensional structure: each $GaSe_4$ tetrahedron connects with an $AsSe_3$ trigonal pyramid by edge sharing to form a $[AsGaSe_5]^{4-}$ cluster (Figure 2b). These $[AsGaSe_5]^{4-}$clusters are further

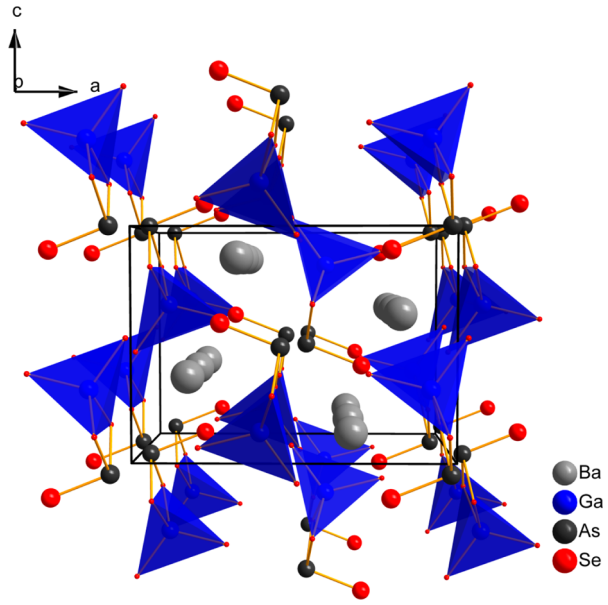

Figure 3. Crystal structure of $Ba_2AsGaSe_5$.

separated by the Ba^{2+} cations, resulting in discrete distribution in the structure. Such an isolated cluster consisting of edge-sharing $GaSe_4$ tetrahedra and $AsSe_3$ trigonal pyramids has been observed for the first time. The $GaSe_4$ tetrahedra are the main functional groups in a number of nonlinear optical materials, including $BaGa_4Se_7$ and $AgGaSe_2$,[38] while the $AsSe_3$ trigonal pyramids are also the main contributors to the nonlinear optical properties in $NaAsSe_2$[39] and Tl_3AsSe_3.[40] The combined $[AsGaSe_5]^{4-}$ anion may be a new kind of nonlinear optically active structural unit, within which the interplay of the $GaSe_4$ tetrahedra and $AsSe_3$ trigonal pyramids may increase the NLO properties. Although the title compound adopts a centrosymmetric structure and the contribution of $[AsGaSe_5]^{4-}$ anions to NLO properties are annulled by the inversion center, chances are high that $[AsGaSe_5]^{4-}$ anions may be found in other noncentrosymmetric structures and lead to increased NLO properties.

Some other compounds with a similar stoichiometry have been obtained, such as Ba_2GaMQ_5 (M = Sb, Bi; Q = Se, Te), $Ba_2InSbTe_5$, and $Ba_2InSbSe_5$.[37] Among them, $Ba_2InSbSe_5$ belongs to the noncentrosymmetric polar space group $Cmc2_1$, while the other five crystallize in the same space group as $Ba_2GaAsSe_5$ (*Pnma*). However, due to the much larger size of Sb and Bi, the Sb or Bi atoms are coordinated to heavily distorted octahedra of six Q atoms in those Sb- or Bi-containing compounds. Furthermore, these MQ_6 octahedra connect with $(Ga/In)Q_4$ tetrahedra, leading to infinite 1-D $^{\infty}_{1}[GaSbQ_5]^{4-}$ or $^{\infty}_{1}[InSbQ_5]^{4-}$ anionic chains, which is in contrast with the isolated $[GaAsSe_5]^{4-}$ anions in $Ba_2GaAsSe_5$.

DOI: 10.1021/acs.inorgchem.5b01501
Inorg. Chem. 2015, 54, 9785−9789

Experimental Band Gap. Figure 4 shows the diffuse reflectance spectrum of $Ba_2AsGaSe_5$. Through an absorption

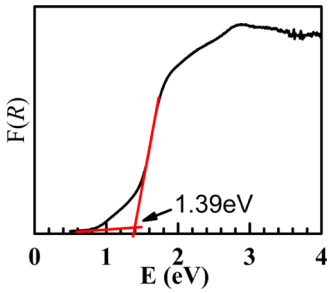

Figure 4. Diffuse reflectance spectrum of $Ba_2AsGaSe_5$.

edge and the linear part of absorption plot, the band gap of $Ba_2AsGaSe_5$ is deduced as 1.39 eV by a straightforward extrapolation method.[33] This value agrees with the black color of the crystal.

Photocatalytic Activities and Investigation of the Mechanism. Photodegradation of the dye Rhodamine B (RhB) is usually utilized to evaluate photocatalytic activity. For the sake of comparison, the important photocatalyst P25 was used for reference. Figure 5 displays the photodecomposition

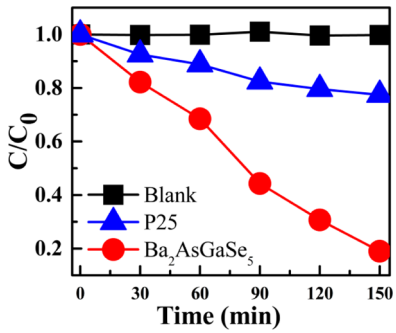

Figure 5. Photocatalytic degradation curves of RhB in the presence of $Ba_2AsGaSe_5$.

curves of RhB over the obtained $Ba_2AsGaSe_5$ and P25 under visible light irradiation (λ >420 nm). Obviously, RhB is stable and photolysis can be ignored. Over 2.5 h of illumination, it can be seen that only 23% of RhB can be degraded over P25. In contrast, $Ba_2AsGaSe_5$ exhibits a highly efficient photocatalytic activity, which can remove almost 81% of the RhB in the same period.

In order to quantitatively study the reaction kinetics during the photodegradation process of RhB, the pseudo-first-order model was fitted on the basis of the Langmuir–Hinshelwood (L–H) kinetics model:[41]

$$\ln(C_0/C) = k_{app}t \quad (1)$$

Here, C_0 represents the initial RhB concentration (mol/L), C is the instantaneous concentration at time t (mol/L), and k_{app} is the apparent pseudo-first-order rate constant (h^{-1}). Figure 5 shows that the corresponding apparent rate constants are 0.6643 and 0.1025 for $Ba_2AsGaSe_5$ and P25, respectively. In other words, the photocatalytic activity of $Ba_2AsGaSe_5$ is 6.5 times higher than that of P25. $Ba_2AsGaSe_5$ is much more effective in photocatalytic degradation of RhB than the previously reported $Dy_4S_4Te_3$, whose photocatalytic performance is just comparable to that of P25.[42]

The occurrence of organic molecule photodegradation is attributed to photo-oxidation by the active radical species generated during the photoreaction process. Under the irradiation of photons with energy high enough to promote the transition of electron across the band gap of the semiconducting photocatalyst, the electron (e^-)–hole (h^+) pairs will result. After jumping to the conduction band, the electrons can further react with O_2 molecules adsorbed on the surface of photocatalysts to form superoxide radicals ($^\bullet O_2^-$) with powerful oxidization. Meanwhile, holes can oxidize the OH^- ions in solution and generate reactive hydroxyl radicals ($^\bullet OH$). $^\bullet O_2^-$, h^+ and $^\bullet OH$ can all act as crucially active species in the photo-oxidation process.

CONCLUSION

$Ba_2AsGaSe_5$ has been synthesized by a conventional solid state reaction, crystallizing in the space group *Pnma*. The discrete novel anion $[AsGaSe_5]^{4-}$, formed by edge-sharing $AsSe_3$ trigonal pyramids and $GaSe_4$ tetrahedra, is observed for the first time. UV–vis–NIR spectroscopy measurements indicate that $Ba_2AsGaSe_5$ has an optical band gap of 1.39 eV. Moreover, $Ba_2AsGaSe_5$ exhibits high visible-light-induced photocatalytic reactivity, which is 6.5 times higher than that of P25. The superoxide radicals ($^\bullet O_2^-$) and photogenerated holes (h^+) play crucial roles in the degradation of RhB, serving as the main active species.

ASSOCIATED CONTENT

Supporting Information

The Supporting Information is available free of charge on the ACS Publications website at DOI: 10.1021/acs.inorgchem.5b01501.

Crystallographic data for $Ba_2AsGaSe_5$ (CIF)

AUTHOR INFORMATION

Corresponding Author

*E-mail for J.Y.: jyao@mail.ipc.ac.cn.

Notes

The authors declare no competing financial interest.

ACKNOWLEDGMENTS

This research was supported by the National Natural Science Foundation of China (Nos. 91122034 and 21271178).

REFERENCES

(1) Zhang, X.; Kanatzidis, M. G.; Hogan, T.; Kannewurf, C. R. *J. Am. Chem. Soc.* **1996**, *118*, 693–694.
(2) Banerjee, S.; Szarko, J. M.; Yuhas, B. D.; Malliakas, C. D.; Chen, L. X.; Kanatzidis, M. G. *J. Am. Chem. Soc.* **2010**, *132*, 5348–5350.
(3) Zhang, F.; Wang, J.; Becker, U.; Lian, J.; Hu, J.; Saxena, S.; Ewing, R. C. *J. Am. Chem. Soc.* **2007**, *129*, 13923–13926.
(4) Ren, P.; Qin, J.; Chen, C. *Inorg. Chem.* **2003**, *42*, 8–10.
(5) Guo, S.-P.; Wang, G.-E.; Zhang, M.-J.; Wu, M.-F.; Liu, G.-N.; Jiang, X.-M.; Guo, G.-C.; Huang, J.-S. *Dalton Trans.* **2013**, *42*, 2679–2682.
(6) Guo, S. P.; Guo, G. C. *J. Mater. Chem. A* **2014**, *2*, 20621–20628.
(7) Mikhailova, D.; Reichel, P.; Tsirlin, A. A.; Abakumov, A. M.; Senyshyn, A.; Mogare, K. M.; Schmidt, M.; Kuo, C.-Y.; Pao, C.-W.; Pi, T.-W.; Lee, J.-F.; Hu, Z.; Tjeng, L. H. *Dalton Trans.* **2014**, *43*, 13883–13891.

DOI: 10.1021/acs.inorgchem.5b01501
Inorg. Chem. 2015, 54, 9785–9789

(8) Zheng, Z.-P.; Zhang, X.-X.; Li, T.; Yang, J.; Wei, L.-M.; Zhang, L.-G.; Lin, X.-M.; Cai, Y.-P. *Dalton Trans.* **2014**, *43*, 14009−14015.
(9) Hong, X.-J.; Liu, X.; Zhang, J.-B.; Lin, C.-L.; Wu, X.; Ou, Y.-J.; Yang, J.; Jin, H.-G.; Cai, Y.-P. *CrystEngComm* **2014**, *16*, 7926−7932.
(10) Luo, Z.-Z.; Lin, C.-S.; Zhang, W.-L.; Zhang, H.; He, Z.-Z.; Cheng, W.-D. *CrystEngComm* **2014**, *16*, 2788−2794.
(11) Kamihara, Y.; Hiramatsu, H.; Hirano, M.; Kawamura, R.; Yanagi, H.; Kamiya, T.; Hosono, H. *J. Am. Chem. Soc.* **2006**, *128*, 10012−10013.
(12) Liu, M. L.; Wu, L. B.; Huang, F. Q.; Chen, L. D.; Ibers, J. A. *J. Solid State Chem.* **2007**, *180*, 62−69.
(13) Yanagi, H.; Tate, J.; Park, S.; Park, C. H.; Keszler, D. A. *Appl. Phys. Lett.* **2003**, *82*, 2814−2816.
(14) Konig, H.; Hoppe, R. *Z. Anorg. Allg. Chem.* **1977**, *434*, 225−232.
(15) Kang, D. H.; Schleid, T. *Z. Anorg. Allg. Chem.* **2009**, *635*, 2170−2176.
(16) Thiele, G.; Rotter, H. W.; Schmidt, K. D. *Z. Anorg. Allg. Chem.* **1987**, *545*, 148−156.
(17) Srinivasan, B. R.; Naether, C.; Bensch, W. *Acta Crystallogr., Sect. E: Struct. Rep. Online* **2007**, *63*, i167.
(18) Yao, J. Y.; Ibers, J. A. *Acta Crystallogr., Sect. E: Struct. Rep. Online* **2004**, *60*, i10.
(19) Mei, D.; Yin, W.; Lin, Z.; He, R.; Yao, J.; Fu, P.; Wu, Y. *J. Alloys Compd.* **2011**, *509*, 2981−2985.
(20) Eisenmann, B.; Jakowski, M.; Schafer, H. *Rev. Chim. Miner.* **1984**, *21*, 12−20.
(21) Wells, D. M.; Ibers, J. A. *Z. Anorg. Allg. Chem.* **2010**, *636*, 440−442.
(22) Chen, C. T.; Wu, B. C.; Jiang, A. D.; You, G. M. *Scientia Sinica Series B* **1985**, *28*, 235−243.
(23) Huang, F. Q.; Ibers, J. A. *Angew. Chem., Int. Ed.* **2001**, *40*, 2515−2516.
(24) Ward, M. D.; Klingsporn, J. M.; Ibers, J. A. *Inorg. Chem.* **2013**, *52*, 10220−10222.
(25) Ward, M. D.; Pozzi, E. A.; Lee, M.; Van Duyne, R. P.; Choi, E. S.; Ibers, J. A. *Inorg. Chem.* **2015**, *54*, 3055−3060.
(26) Chung, I.; Jang, J. I.; Gave, M. A.; Weliky, D. P.; Kanatzidis, M. G. *Chem. Commun.* **2007**, *47*, 4998−5000.
(27) (a) Xiong, W.-W.; Miao, J.; Ye, K.; Wang, Y.; Liu, B.; Zhang, Q. *Angew. Chem., Int. Ed.* **2015**, *54*, 546−550. (b) Xiong, W. W.; Athresh, E. U.; Ng, Y. T.; Ding, J. F.; Wu, T.; Zhang, Q. C. *J. Am. Chem. Soc.* **2013**, *135*, 1256−1259. (c) Xiong, W. W.; Li, P. Z.; Zhou, T. H.; Tok, A. L. Y.; Xu, R.; Zhao, Y. L.; Zhang, Q. C. *Inorg. Chem.* **2013**, *52*, 4148−4150. (d) Xiong, W.-W.; Zhang, G.; Zhang, Q. *Inorg. Chem. Front.* **2014**, *1*, 292−301.
(28) Reshak, A. H.; Auluck, S. *Opt. Mater.* **2014**, *38*, 80−86.
(29) (a) Huang, H. W.; Wang, J. J.; Dong, F.; Guo, Y. X.; Tian, N.; Zhang, Y. H.; Zhang, T. R. *Cryst. Growth Des.* **2015**, *15*, 534−537. (b) He, Y.; Huang, H. W.; Zhang, Y. H.; Li, X. W.; Tian, N.; Guo, Y. X.; Luo, Y. *Mater. Res. Bull.* **2015**, *64*, 405−409.
(30) Huang, F. Q.; Wu, J. J.; Lin, X. P.; Zhou, Z. *J. Alloys Compd.* **2011**, *509*, 764−768.
(31) *CrystalClear*; Rigaku Corp., Tokyo, Japan, 2008.
(32) Sheldrick, G. M. *Acta Crystallogr., Sect. A: Found. Crystallogr.* **2008**, *64*, 112−122.
(33) Schevciw, O.; White, W. B. *Mater. Res. Bull.* **1983**, *18*, 1059−1068.
(34) Mei, D.; Yin, W.; Bai, L.; Lin, Z.; Yao, J.; Fu, P.; Wu, Y. *Dalton Trans.* **2011**, *40*, 3610−3615.
(35) Cordier, G.; Schwidetzky, C.; Schafer, H. *Inorg. Chem. React.* **1985**, *22*, 93.
(36) Feng, K.; Jiang, X. X.; Kang, L.; Yin, W. L.; Hao, W. Y.; Lin, Z. S.; Yao, J. Y.; Wu, Y. C.; Chen, C. T. *Dalton Trans.* **2013**, *42*, 13635−13641.
(37) Hao, W.; Mei, D.; Yin, W.; Feng, K.; Yao, J.; Wu, Y. *J. Solid State Chem.* **2013**, *198*, 81−86.
(38) Tell, B.; Kasper, H. M. *Phys. Rev. B* **1971**, *4*, 4455.
(39) Bera, T. K.; Jang, J. I.; Song, J. H.; Malliakas, C. D.; Freeman, A. J.; Ketterson, J. B.; Kanatzidis, M. G. *J. Am. Chem. Soc.* **2010**, *132*, 3484−3495.
(40) Hong, H. Y. P.; Mikkelsen, Jc; Roland, G. W. *Mater. Res. Bull.* **1974**, *9*, 365−369.
(41) Huang, H. W.; He, Y.; Lin, Z. S.; Kang, L.; Zhang, Y. H. *J. Phys. Chem. C* **2013**, *117*, 22986−22994.
(42) Guo, S.-P.; Guo, G.-C. *J. Mater. Chem. A* **2014**, *2*, 20621−20628.

DOI: 10.1021/acs.inorgchem.5b01501
Inorg. Chem. 2015, 54, 9785−9789